A setup for vacuum-ultraviolet spectroscopy of the ^{229}Th low-energy isomer

Sandro Kraemer[a,b,*], Premaditya Chhetri[a], Silvia Bara[a], Arno Claessens[a], Hilde De Witte[a], Yens Elskens[a], Rafael Ferrer[a], Yuri Kudryavtsev[a], Simon Sels[a], Paul Van Den Bergh[a], Piet Van Duppen[a]

[a] *KU Leuven, Instituut voor Kern- en Stralingsfysica, Celestijnenlaan 200D, 3001, Leuven, Belgium*
[b] *Ludwig-Maximilians-Unversität München, Fakultät für Physik, Am Coulombwall 1, 85748, Garching, Germany*

Abstract

The ground-state transition of the low-energy isomer in ^{229}Th has been proposed as the basis for the development of a novel optical clock as a tool for fundamental-physics studies. Vacuum-ultraviolet studies of the β-decay of ^{229}Ac recently enabled to measure the de-excitation energy of the isomer with a seven-fold improvement in precision compared to previous results by directly observing photons from the isomer's radiative decay. In this contribution, the setup used for this study and the systematic uncertainty on the measured photon wavelength is discussed.

Keywords: isomer, thorium-229, nuclear clock, vacuum-ultraviolet spectroscopy
PACS: 21.10.-k, 0706Rd

A unique feature of the radioisotope ^{229}Th is its low-energetic isomer at approximately 8 eV. Such a small excitation energy potentially allows for direct laser manipulation of nuclear states and has been proposed as the base for a new optical clock based on a nuclear transition [1]. Such a future metrology instrument offers unique opportunities as a very sensitive quantum sensor for fundamental-physics measurements such as temporal variations of the fine structure constant and in the search for specific types of ultralight topological dark matter [2–4]. Although first evidence for such an extraordinary nuclear state stems from almost 50 years ago, the first direct detection has been achieved only recently [5] by populating the isomer in the α-decay of ^{233}U. A series of measurements using the detection of conversion electrons, the hyperfine interaction with the electron shell and employing precise gamma-spectroscopy have been used to further characterize the properties of this state [6–10].

The radiative decay of the isomeric state, located in the vacuum-ultraviolet (VUV) region of the electromagnetic spectrum, competes directly with the electron conversion decay and has recently been observed for the first time by populating the isomer in the β-decay of ^{229}Ac[11]. The study allowed to measure the excitation energy of the isomer with an seven-fold improvement in uncertainty compared to previous results and enabled to determine an estimate of the lifetime of the ^{229m}Th embedded in a magnesium-fluoride crystal.

In this work, vacuum-ultraviolet spectroscopy of the photons emitted after the β-decay of ^{229}Ac measures the wavelength of photons from the isomer's radiative decay, which can directly be related to its excitation energy. Radioisotope beams of mass $A = 229$ produced at the ISOLDE-CERN facility by a 1.4 GeV proton beam impinging on a uranium carbide target are implanted into large-bandgap calcium- and magnesium fluoride crystals. The crystals are mounted on a target wheel and radioactivity is monitored by a high-purity germanium γ-detector located close to the implantation position of the crystal. After implantation of the radioactive beam consisting predom-

*Corresponding author (sandro.kraemer@physik.uni-muenchen.de)

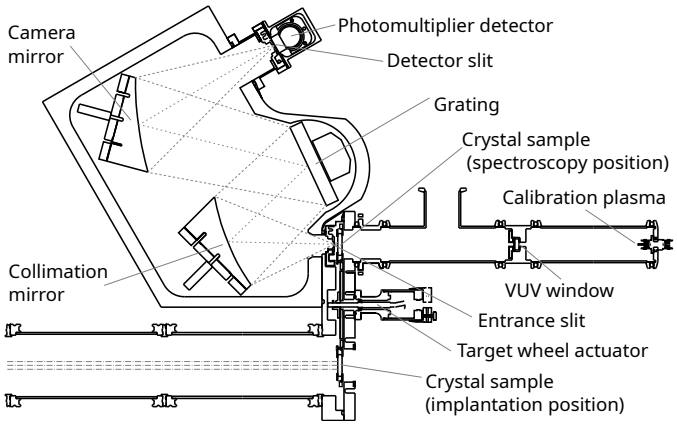

Figure 1: The VUV-spectroscopy setup. The symmetry axis and the envelope of the light path and the ion beam are shown as a dashed and dash-dotted line, respectively.

inantly of ^{229}Fr and ^{229}Ra, the target wheel is rotated by 180 degrees and the crystal is placed with a 3 mm distance in front of the entrance slit of the grating monochromator (Resonance Ltd. VM180). Two off-axis parabolic mirrors in a Czerny-Turner mount lead to a high numerical aperture of F/1.2 for light sources at the entrance slit. The emitted light spectrum are recorded with a solar-blind photomultiplier tube (Hamamatsu R8487), located behind the detector slit, by scanning the angle of the plane diffraction grating with a groove density of 4000 mm^{-1} (c.f. Fig. 1). The grating angle is set by a crankshaft from a linear motor position x. The central wavelength is obtained from the motor position by a linear calibration relation.

Figure 2 shows the photon detection rate as a function of wavelength λ normalized per ^{229}Ac decay in a 5 mm thick MgF_2 (red), a 5 mm thick CaF_2 (blue) and a 50 nm thick thin-film CaF_2 crystal sample (for details, see [11]). The momentous activity of the implanted ^{229}Fr-, ^{229}Ra- and ^{229}Ac nuclei are calculated using Bateman-equations from the measured activity during the implantation period. The continuous background in the case of the 5 mm-thick crystal samples is induced by fast electrons as Cherenkov radioluminescence. The radiative decay of the ^{229m}Th isomer populated in the decay of ^{229}Ac is visible as a peak around 148 nm in all three crystal samples. In thick CaF_2 an additional peak from a crystal defect is visible around 183 nm (c.f. [11] for a discussion).

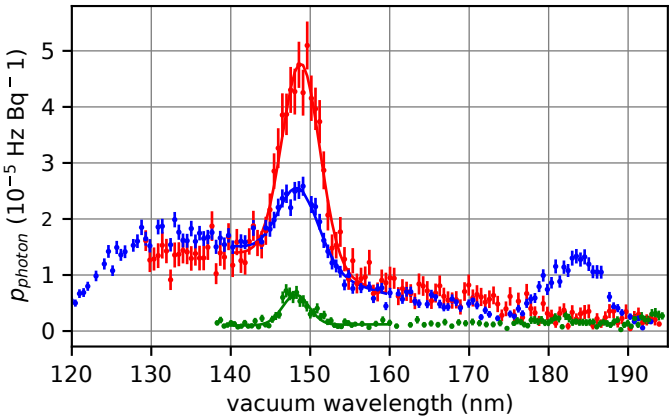

Figure 2: Photon detection probability per decay of ^{229}Ac as a function of wavelength for the implantation of a beam of A=229 into a 5 mm thick crystal of MgF_2 (red), a 5 mm thick crystal of CaF_2 (blue) and a 50 nm thick thin-film crystal of CaF_2 (green). The observed photon count rate has been recorded with a 3 mm entrance slit and is normalized to the activity deduced from γ-data recorded during implantation.

Measured wavelength spectra are obtained by scanning the wavelength from lower to higher values and recording the count rate on the photomultiplier detector for 10 to 30 s per wavelength setting. Wavelength spectra consist of a Gaussian peak from the monochromatic isomer's radiative decay on top of the continuous Cherenkov-radioluminesence background. The emitted spectrum is shaped by the instrument's and crystals wavelength-dependent transmission efficiency and approximated by a third-order polynomial obtained experimentally from a reference measurements in the $A = 230$ β-decay chain. The centroid of the isomer's radiative decay signal is reached after 1.17 h, 1.18 h and 1.05 h for the 5 mm MgF_2, the 5 mm CaF_2 and the 50 nm CaF_2 crystal, such that an activity equilibrium between the actinium and the thorium isomer activity can be assumed. The change of activity during the recording of the wavelength spectrum is taken into account by scaling the Gaussian peak as well as the Cherenkov-radioluminescence background with the inverse of an exponential decay of the actinium half-life $T_{1/2} = 62.7$ min. Obtained fits scaled by the activity are shown in Fig. 2.

The observed fractional photon creation probabilities p_{photon} per ^{229}Ac decay can be defined as

$$p_{\text{photon}} = \epsilon_{\text{feeding}} \cdot \epsilon_{\text{rad.decay}} \cdot \epsilon_{\text{coll.+det.}}(\lambda), \quad (1)$$

where λ is the wavelength of photons emitted in the radiative decay. It consists of the decay-specific isomer feeding efficiency $\epsilon_{\text{feeding}}$ (β-decay branching ratio towards the isomer) of the ^{229}Ac decay. This quantity is not exactly known and expected in the range between $0.14 \leq \epsilon_{\text{feeding}} \leq 0.93$ [11, 12]. For a populated isomeric state to deexcite via the radiative decay channel, the nucleus has to occupy a suitable crystal lattice position. The fraction of nuclei in such a position $\epsilon_{\text{rad.decay}}$ is likewise unknown, but emission channeling measurements hint to a significant fraction [11]. The instrument- and crystal-sample-specific photon collection and detection efficiency $\epsilon_{\text{coll.+det.}}(\lambda)$ is composed of the monochromator's transmission efficiency and the quantum efficiency of the detector with typically $\approx 9.8 \cdot 10^{-4}$. Additionally, the transmission of photons from the implanted nuclei in the crystal to the surface and from there to the entrance slit has to be taken into account and depends on the crystal material and surface as well as on the implantation distribution on the crystal (A typical distribution root-mean-square is $\geq 5\,\text{mm}$ and is to be compared to a rectangular slit of $3\,\text{mm} \times 10\,\text{mm}$ at a distance of 3 mm) and the exact sample holder wheel position with respect to the entrance slit. These contributions are unknown and are expected to vary between different spectra in Fig. 2, impeding a quantitative analysis of $\epsilon_{\text{feeding}}$ for different crystal materials. The observed p_{photon} in the spectra shown in fig. 2 are $3.60(17) \cdot 10^{-5}$ (5 mm thick MgF_2), $1.34(8) \cdot 10^{-5}$ (5 mm thick CaF_2) and $5.0(4) \cdot 10^{-6}$ (50 nm thick CaF_2), respectively. The given error represents the uncertainty from the fit and excludes systematic uncertainty.

For the measurement of photon wavelengths, highest accuracy is achieved with a diffraction-limited entrance slit opening, at the same time reducing significantly the count rate for a given isotropic photon flux from a spatially distributed source of implanted nuclei. Slit sizes between 0.25 mm and 0.5 mm are used as a trade-off between reduced systematic wavelength uncertainties and sufficient transmission with achievable ^{229}Ac source strengths. For photons crossing the plane of the entrance slit at a lateral distance Δy from its center, a shift of $\Delta\lambda/\Delta y = 1.33\,\text{nm}\,\text{mm}^{-1}$ is observed due to the change in incidence angle on the grating. For a 0.5 mm(0.25 mm) slit opening this translates thus to a conservative systematic uncertainty due to the uknown implantation distribution on the wavelength λ of $\leq$ 0.33 nm (0.17 nm).

Multiplet	Atomic transition(s)	Element
130.37 nm	130.2168 nm	O(I)
	130.4858 nm	
	130.6029 nm	
141.194 nm	141.194 nm	N(I)
149.34 nm	149.2625 nm	N(I)
	149.2820 nm	
	149.4675 nm	
174.39 nm	174.2731 nm	N(I)
	174.5249 nm	

Table 1: List of atomic multiplets in a nitrogen-oxygen plasma used for the wavelength calibration of the grating drive. The corresponding atomic transitions and the element and charge state in the plasma are given [13].

An external nitrogen-oxygen plasma source, mounted on the optical axis of the monochromator entrance slit at a distance of 350 mm, is used to calibrate the grating motor drive position x in terms of wavelength λ. Table 1 lists three non-resolvable multiplets fitted with a Lorentzian lineshape, and attributed with an intensity-weighted average of the composing atomic transitions, as well as one single transition that are used for calibration [13]. Figure 3 shows a typical calibration spectrum. From nine different spectra, recorded using a 10 µm entrance slit during two different periods with an interval of three months in between, a calibration relation

$$\lambda(x) = 146.755(25)\text{nm} + 0.008684(11)\text{nm} \cdot x \quad (2)$$

is obtained.

A second systematic offset has to be taken into account in case the axis of the calibration source,

on which the plasma and the exit window of the source lie, is not aligned with the optical axis formed by the centers of the entrance slit opening and the collimation mirror. For deviations of up to ± 1 mm, an additional systematic uncertainty of ≤ 0.15 nm has to be added.

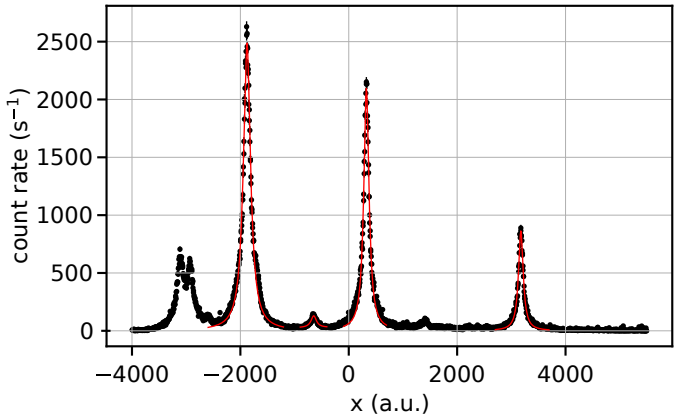

Figure 3: Typical calibration spectrum recorded with a 10 µm entrance slit. A fit of the four lines used for the spectrometer calibration are shown.

The crankshaft grating drive introduces a third systematic uncertainty through its intrinsic reproducibility. Using a large amount of repeated measurements of the positions of the calibration peaks with varying scanning ranges, the remaining systematic uncertainty of the grating drive is estimated to be ≤ 0.18 nm.

The statistical uncertainty of the measured wavelength is composed of the uncertainty obtained from the fit and the uncertainty introduced during wavelength calibration with equation 2. Additionally, systematic uncertainties of 0.41 nm (0.29 nm) for an entrance slit width of 0.5 mm (0.25 nm) have to be taken into account.

In summary, the vacuum-ultraviolet spectroscopy instrument presented here has been used for the first observation of the radiative decay of the ^{229}Th low-energy isomer. In a series of experiments at the ISOLDE facility the technique enabled not only to identify a signal as the effect of the isomeric decay but also to improve significantly the uncertainty on the isomer's excitation energy by measuring the wavelength of the emitted photons. Ongoing technical developments should, on the one hand, further reduce the systematic uncertainty of the measured wavelength to allow for more precise measurements and, on the other hand, reduce the uncertainty on the collection and detection efficiency $\epsilon_{\text{coll.+det.}}$ to enable studies comparing $\epsilon_{\text{rad.decay}}$ in different crystal materials and using different preparation methods. Future experiments using this technique will contribute paving the way towards a future solid-state nuclear clock.

Acknowledgements

This work was supported by Research Foundation Flanders FWO; FWO and F.R.S.-FNRS [EOS programme nr. 40007501], Marie Skłodowska-Curie Actions [nr. 101026762] and the European Research Council [Thorium Nuclear Clock nr. 856415].

References

[1] E. Peik, C. Tamm, Nuclear laser spectroscopy of the 3.5 eV transition in Th-229, EPL 61 (2) (2003) 181.
[2] A. Derevianko, M. Pospelov, Hunting for topological dark matter with atomic clocks, Nature Physics 10 (12) (2014) 933–936.
[3] P. G. Thirolf, B. Seiferle, L. von der Wense, Improving our knowledge on the ^{229m}Thorium isomer: Toward a test bench for time variations of fundamental constants, Ann. Phys. 531 (5) (2019) 1800381.
[4] E. Peik, T. Schumm, M. S. Safronova, et al., Nuclear clocks for testing fundamental physics, Quantum Sci. Technol. 6 (3) (2021) 034002.
[5] L. von der Wense, B. Seiferle, M. Laatiaoui, et al., Direct detection of the ^{229}Th nuclear clock transition, Nature 533 (7601) (2016) 47–51.
[6] B. Seiferle, L. von der Wense, P. G. Thirolf, Lifetime measurement of the ^{229m}Th nuclear isomer, Phys. Rev. Lett. 118 (4) (2017) 042501.
[7] J. Thielking, M. V. Okhapkin, P. Głowacki, et al., Laser spectroscopic characterization of the nuclear-clock isomer ^{229m}Th, Nature 556 (7701) (2018) 321–325.
[8] B. Seiferle, L. von der Wense, P. V. Bilous, et al., Energy of the ^{229}Th nuclear clock transition, Nature 573 (7773) (2019) 243–246.
[9] A. Yamaguchi, H. Muramatsu, T. Hayashi, et al., Energy of the ^{229}th Nuclear Clock Isomer Determined by Absolute γ-ray Energy Difference, Phys. Rev. Lett. 123 (22) (2019) 222501.
[10] T. Sikorsky, J. Geist, D. Hengstler, et al., Measurement of the ^{229}Th isomer energy with a magnetic microcalorimeter, Phys. Rev. Lett. 125 (14) (2020) 142503.
[11] S. Kraemer, J. Moens, M. Athanasakis-Kaklamanakis, et al., Observation of the radiative decay of the ^{229}Th nuclear clock isomer (2022). doi:10.48550/ARXIV.2209.10276.
[12] M. Verlinde, S. Kraemer, J. Moens, et al., Alternative approach to populate and study the ^{229}Th nuclear clock isomer, Phys. Rev. C 100 (2) (2019) 024315.
[13] Y. Ralchenko, A. Kramida, Development of nist atomic databases and online tools, Atoms 8 (3) (2020) 56.